Breakup of Liquid Sheets and Jets in a Supersonic Gas Stream

ALLAN SHERMAN*
NASA Goddard Space Flight Center, Greenbelt, Md.
AND
JOSEPH SCHETZ†
Virginia Polytechnic Institute, Blacksburg, Va.

Experimental and analytical results are presented with the objective of defining the mechanism of liquid sheet and jet breakup when subjected to a supersonic gas stream. Liquid sheets are studied with photomicrographs and high-speed movies of the activity of a liquid layer maintained upon a porous plate test model in a parallel Mach 2.2 freestream. Tests with several different liquids show wave motion, with droplet and ligament shedding across the liquid surface. Numerical results from a liquid surface stability analysis are used to explain these observations. Liquid jets are studied with spark shadowgraphs, high-speed movies and photomicrographs of the normal injection of various liquids into a Mach 2.1 freestream. The results show that the breakup mechanism is characterized by gross jet fracture, as opposed to surface disintegration. The degree of breakup at a given streamwise location and jet spread after injection are found to be related to injection diameter and dynamic pressure, and certain liquid properties.

Nomenclature

C_f = skin friction coefficient
ΔN = fraction of droplets counted between $X_{\min}$ and $X_{\max}$
ΔX = droplet diameter increment
g = acceleration of gravity
G = defined by Eq. (3)
G^* = defined by Eqs. (5) and (7)
K = wave number $= 2\pi/\lambda$
M = Mach number
$\dot{m}$ = liquid mass flow rate
n = constant defined by Eq. (1)
q_r = dynamic pressure ratio $= \rho_l V_J^2/\rho_g U^{*2}$
Re = denotes real part
T = liquid surface tension
t = time independent variable
U^* = freestream velocity
U_g = perturbation velocity from "wavy wall" solution from linearized theory
u_g = x component of gas velocity
u_l = x component of liquid velocity
v_g = y component of gas velocity
V_J = liquid injection velocity
v_l = y component of liquid velocity
x = space independent variable
X = droplet diameter (droplet distribution graphs)
$X_{\min}$ = lower limit of droplet diameter increment
$X_{\max}$ = upper limit of droplet diameter increment
y = space independent variable
$\bar{y}$ = defined by Eq. (1)
Z = defined by Eqs. (6) and (8)
β = sheltering parameter
λ = wavelength
λ_c = minimum wavelength for growth
λ_M = wavelength for maximum growth
μ_g = gas viscosity
μ_l = liquid viscosity
ν_l = liquid kinematic viscosity
ρ_g = gas density
ρ_l = liquid density
τ_0 = surface shear stress
ξ = $i(n/K^2\nu_l)$

Received January 26, 1971; revision received October 6, 1970. This work was supported in part by the Propulsion Division, Air Force Office of Scientific Research under Grant AF-AFOSR-1228-67, Mod. AFOSR-67-1228A, Project Task 9711-01 with Technical Supervision by B. T. Wolfson.

* Staff Engineer, Engineering Physics Division.
† Professor and Chairman, Aerospace Engineering. Associate Fellow AIAA.

I. Introduction

MANY early investigators were interested in the interfacial activity between two superposed fluid streams.[1-5] In more recent years, analytical and experimental investigations have concentrated in describing the surface stability and activity of a liquid over which a gas stream flows. Of particular importance in the regime of high freestream velocity is the analysis of Mayer,[6] in which a model for droplet shedding from unstable surface waves is presented, and Chang and Russel,[7] in which linearized theory is employed to develop wave stability criteria with subsonic and supersonic freestream velocities.

Most of the investigations into the breakup of liquid jets have been limited to injection into still media,[8-12] or a determination of downstream droplet sizes after injection into a subsonic freestream.[13,14] Studies as to the mechanism of jet breakup after injection into a gaseous freestream have been limited to Clark,[15] who, for a subsonic gas stream, proposed a breakup model of a flattened liquid stream with drops and ligaments torn off the edges, and, Adelberg,[16] who proposed, for a high-velocity freestream, a theoretical model in which droplets are shed from surface waves while the jet remains essentially intact. A bibliography of jet injection literature, including articles concerned more with penetration than breakup, is contained in Ref. 17.

The purpose of the present investigation was to determine the basic mechanism of breakup of both liquid sheets and jets, when exposed to a supersonic freestream. To accomplish this objective, spark photomicrographs and high-speed movies were employed to obtain pictures of the activity of a liquid layer maintained upon a porous plate test model in a supersonic freestream, and the breakup of liquid jets injected normally into a supersonic freestream. In addition, spark shadowgraphs were taken for some of the jet injection tests. Theoretical comparisons were limited to the liquid sheet problem in which numerical solutions of the liquid stability analysis of Chang and Russel were correlated with experimental observations.

II. Liquid Sheets

Experimental Studies

The liquid sheet tests were conducted in a 6-in. supersonic wind tunnel of the indraft type with a run time of 15

sec. Measured freestream Mach number was 2.2 for all tests, with a gas velocity of 1770 fps. Gas stagnation pressure and temperature were at atmospheric conditions, with the incoming stream dried via a silica-gel bed dryer attached to the front of the tunnel.

The porous plate model employed for the liquid sheet tests spans the test section of the tunnel, is 7 in. long, $\frac{1}{2}$ in. thick, and has a 20° half wedge angle at the leading edge. There is an initial 1-in. solid portion followed by a 5 in. porous surface and a 1 in. solid trailing edge. The porous plate is $\frac{1}{8}$ in. thick stainless steel powder, with an average pore size of 10 μ, and is approximately 50% void. The plate is attached to the stainless steel base by means of spanwise steps in the solid leading and trailing sections. Liquid is fed into the model settling chamber through small holes in $\frac{3}{8}$ in. o.d. stainless steel tubes running lengthwise under the porous section, and thus a liquid layer is maintained upon the surface of the plate.

Photomicrograph Tests

Optical apparatus

Light from a 0.4 μsec spark source was focused by a 5 in. focal length lens and 5 ft focal length mirror to an image plane halfway across the plate. This image was about 1 in. long and $\frac{1}{4}$ in. high due to the imperfection of the 5 in. focal length lens. Thus, a high intensity light "source" was formed at the liquid-gas interface. A high precision 6-in. focal length lens and iris were then used for magnification and focussing. The camera was operated without its lens, and Polaroid Type 57 (3000 speed) was used throughout the tests.

Test procedure

The test sequence was to initiate liquid flow via a solenoid valve 3 sec prior to tunnel start, and to take the pictures 4 sec after tunnel start. Visual observation, later verified by high-speed movies, showed that steady-state flow conditions had been attained by the time the pictures were taken.

Test liquids

Table 1 lists the six liquids that were tested during this phase of the study. The basis for liquid selection was to provide a wide range of physical properties commensurate with wind-tunnel operation safety standards. The physical properties itemized in the table were obtained from the indicated references for the temperature recorded by plate settling chamber thermocouples at the time the pictures were taken. Although 15 to 20 pictures were taken for each test, the liquid temperature never varied by more than two or three degrees. Thus, an average temperature for each test was used for liquid physical property determination.

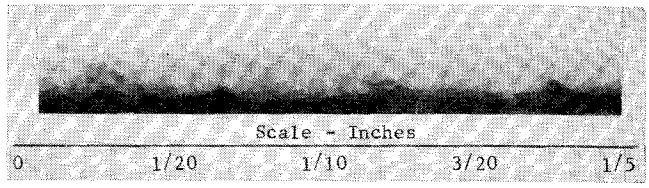

Fig. 1 Liquid sheet test—water.

Results of photomicrograph tests

A sample from the results of the photomicrograph tests is shown in Fig. 1 which is an enlargement of a section of the original photograph. This picture shows the liquid-gas interface with the gas flow from right to left. The salient features of this photograph, as well as other photographs obtained from this phase of testing, are the following: 1) The pictures obtained from this phase of testing show clear evidence of a wave-like type of activity on the liquid surface, accompanied by droplet and ligament shedding. Note in Fig. 1, for example, the shedding of a relatively large liquid ligament (left side of picture), as well as the shedding of a smaller ligament (right of center in the picture), with wave-like protrusions on the liquid surface. 2) The thicknesses of the liquid layers is estimated from the results of these tests to be on the order of 150 μ (0.006 in.). 3) The surface waves do not appear to be of a smooth periodic type. Rather, the waves look like protrusions resembling a sine wave that ends after half of a period. The thickness of these protrusions at the base is on the order of 150 μ, as compared to less than 50 μ for the shedding ligaments. 4) For the carbon tetrachloride test (No. 4) photomicrographs of the surface waves were not obtained. This is hypothesized to be due to a) a large number of closely spaced waves which obscure the activity at the mid-span plane (verified by high-speed movies), b) smaller wave thicknesses as predicted theoretically, and c) rapid evaporation of the carbon tetrachloride at the liquid-gas interface, which works in the direction of preventing the growth of waves of detectable sizes. 5) One photograph from each test was selected for the purpose of counting and measuring droplets. These pictures were taken with the iris in the half-open position. The droplet sizes were measured by examination of the pictures under a microscope with a 5:1 magnification, and a reticle graduated in tenths of millimeters. Thus, the minimum measurable interval was nominally 5 μ, corresponding to half the minimum graduation of the reticle. However, it should be noted that difficulty was encountered in distinguishing the droplets in the 5–10 μ range from the grain of the picture. Furthermore, in measuring the droplet diameters only those droplets in good focus were counted.

A typical example of the droplet distributions obtained is shown in Fig. 2, which is a histogram of the droplet diameters from Test 1. The sample sizes obtained from the photographs for the calculations of these distributions ranged from 38 for Test 5 to 149 for Test 1. Thus, because of these relatively low sample sizes, smooth distributions were not obtained. The results of the droplet distribution determinations show that,

Table 1 Liquid properties for liquid sheet tests[21–24]

Test no.	Liquid	Viscosity, lb_M/ft-sec	Density, lb_M/ft^3	Surface tension, lb/ft	Vapor pressure, MM H_g
1	Water	0.82×10^{-2}	62.4	5.08×10^{-3}	11.7
2	20% glycerol/water solution	1.51×10^{-3}	65.5	4.81×10^{-3}	7.4
3	30% glycerol/water solution	2.48×10^{-3}	67.2	4.82×10^{-3}	7.0
4	Carbon tetrachloride	0.76×10^{-3}	99.0	1.91×10^{-3}	56
5	5% ethyl alcohol/water solution	0.93×10^{-3}	62.2	3.92×10^{-3}	12.8
6	2½% ethyl alcohol/water solution	0.93×10^{-3}	62.2	4.23×10^{-3}	12.6

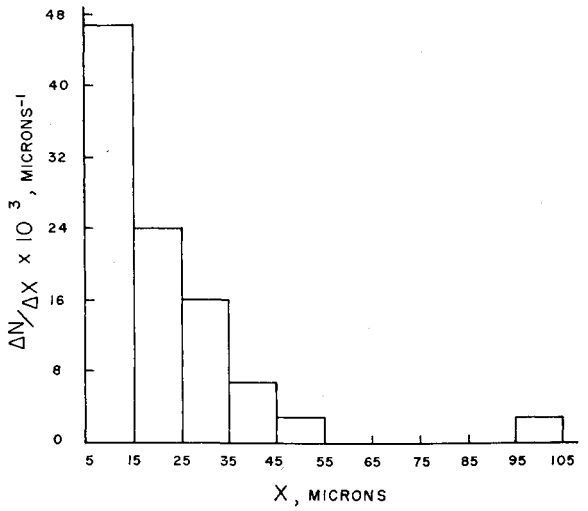

Fig. 2 Liquid sheet droplet distribution—water.

with the exception of carbon tetrachloride, the maximum observed droplet chamber is in the 100 μ range, and the mean measured droplet diameter is between 21 and 31 μ, for each of the liquids tested. For the carbon tetrachloride test the maximum observed droplet diameter was in the 25 μ range and it is estimated that 95% of the observed droplets were 10 μ or less in diam. Furthermore, distribution curves obtained for all of the test liquids were skewed towards the smaller diameter class intervals as illustrated by Fig. 2.

High-speed movies

High-speed movies (16 mm—7000 frame/sec) were taken of a portion of the liquid surface (about 5 in. from the leading edge) for tests with water, carbon tetrachloride, and a 20% glycerol/water solution. These films included steady-state tests for all three liquids in which the camera was started one second after tunnel start and terminated approximately three sec later (corresponding timewise to the spark photomicrograph tests), and one roll of the transient development of the liquid surface with water as the working fluid.

The steady-state movies show quite clearly the wave motion across the surface of the liquid for all three tests. In general, the waves are three-dimensional in nature (i.e., do not span the plate) and progress at a measurable velocity in the streamwise direction along the plate. Also, as discovered with the spark photomicrograph pictures, the waves do not appear to be the usual idealized periodic type, but rather individual protrusions resembling a sine wave terminated after half of a period.

Significant differences in the wave motion among the three fluids tested are also observed in the high-speed movies. First, the carbon tetrachloride liquid layer exhibits a much larger number of closely spaced waves than the glycerol solution, with water somewhere between the two. Second, the thickness at the base of the waves ranges from small to large in comparing the carbon tetrachloride, water, and glycerol solution tests. Third, the wave velocity is noticeably different in observing the wave motion across the surface for the three tests. As measured from the movies these wave velocities averaged 4.9 fps for the carbon tetrachloride test, 8.2 fps for the water test, and 6.1 fps for the test with a 30% glycerol/water solution.

Theoretical Considerations

A stability analysis for the flow of an inviscid compressible gas over a liquid surface was initially presented by Chang and Russel,[7] and later expanded by Wilson and Chang.[18] Lubard and Schetz[19] then obtained a numerical solution to the nondimensional stability equation of Wilson and Chang. In the present investigation this analysis was expanded to determine the effect of gas viscosity with respect to the resulting shear on the surface of the liquid. Numerical solutions were obtained for both the inviscid and viscid gas cases, and the solutions for the inviscid gas case were employed to explain the experimental results. In addition, these solutions were compared with the other basic approach to the problem, i.e. the "sheltering parameter" method presented by Mayer.

Analysis with Gas Viscosity

The details of this analysis can be obtained from Ref. 17. In general, the analysis follows the Chang and Russel approach of assuming an infinite liquid depth, linearized form of the momentum equation, two-dimensional flow, and that the pressure distribution imposed by the gas is determined by the "wavy wall" solution from linearized theory. With these assumptions, and assuming a periodic disturbance on the liquid surface,

$$\bar{y} = Re[\eta e^{iKx-int}] \tag{1}$$

the momentum and continuity equations can be solved for the liquid velocity components and pressure in terms of four complex constants.

Now, the new interfacial shear conditions at $y = 0$ are

$$\mu l\left(\frac{\partial ul}{\partial y} + \frac{\partial vl}{\partial x}\right) = \mu_g\left(\frac{\partial u_g}{\partial y} + \frac{\partial v_g}{\partial x}\right) \approx \mu_g \frac{\partial u_g}{\partial y} \tag{2}$$

and

$$\left.\frac{\partial u_g}{\partial y}\right|_{y=0} \equiv U_g G(x,t) \tag{3}$$

where $G(x,t)$ is an arbitrary function of position and time at our disposal. By substituting the expressions for the velocity components and combining Eqs. (2) and (3) a relationship between the unknown constants is obtained which is then combined with an expression for the liquid surface normal stress.

The analysis now again follows that of Chang and Russel in which expressions for the liquid interfacial normal stress, sur-

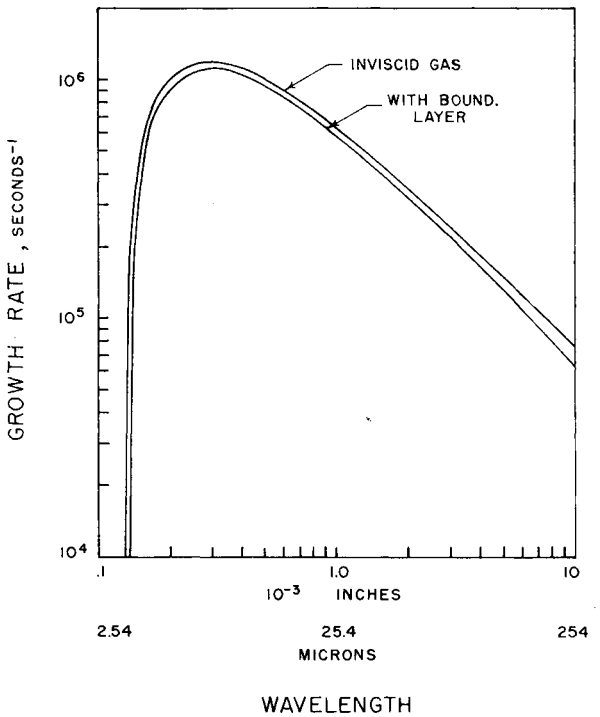

Fig. 3 Effect of gas boundary layer on liquid stability curves.

face tension, and gas pressure, are equated to the normal acceleration at the interface. The resulting stability equation is

$$(4 - 2G^*)(1 - \xi)^{1/2} - (\xi - 2)^2 + 2G^*/\xi = Z + G^* \quad (4)$$

where for a subsonic freestream

$$G^* = 2\mu_g GU^* i/[\rho l K^2 \nu l^2 (1 - M^2)^{1/2}] \quad (5)$$

$$Z = \frac{[Kg + K^3 T/\rho l] - \{[K^2/(1 - M^2)^{1/2}](\rho_g/\rho l)U^{*2}\}}{K^4 \nu l^2} \quad (6)$$

and for a supersonic freestream

$$G^* = 2\mu_g GU^*/[\rho l K^2 \nu l^2 (M^2 - 1)^{1/2}] \quad (7)$$

$$Z = \frac{\left[Kg + \frac{K^3 T}{\rho l}\right] + i\left[\frac{K^2}{(M^2 - 1)^{1/2}}\left(\frac{\rho_g}{\rho l}\right)U^{*2}\right]}{K^4 \nu l^2} \quad (8)$$

It should be noted that if the gas viscosity is taken as zero Eq. (4) reduces to the inviscid gas case of Chang and Wilson. Also, at this point we are restricting ourselves to a constant value for G. It is now desirable to obtain solutions to Eq. (4), i.e., obtain the wavelengths of the initial disturbances for which there is a positive imaginary value for n, indicating initial perturbation growth.

Numerical Results

In order to obtain a solution to Eq. (4) it is necessary to estimate a constant value for G which best represents the fluctuating interfacial shear. In order to do this we say

$$\tau_0 = \overline{\mu_g G(x,t)}\bar{U}_g = C_f \tfrac{1}{2}\rho_g U^{*2} \quad (9)$$

or

$$\overline{\mu_g G} = C_f \tfrac{1}{2}\rho_g U^*(U^*/\bar{U}_g) \quad (10)$$

where $\bar{U}_g$ is some average perturbation velocity and $\mu_g G$ is now a constant to be used in calculating G^*. C_f was taken as that for a flat plate with laminar flow,[20] and various values of $U^*/\bar{U}_g$ were assumed in the computations.

Figure 3 shows the results of the computation for $U^*/\bar{U}_g = 10$, with the fluid properties and test conditions of Test 4. Plotted in Fig. 3 is a curve of wave growth rate vs wavelength obtained from the solution of Eq. (4), for which there is a positive wave growth. Only one such solution was found to exist for each wavelength. The second curve in Fig. 3 is the inviscid gas solution to Eq. (4) for the fluid properties and test conditions of Test 4. Comparison of the curves shows that the addition of the gas shear has little effect on either the shape or magnitude of the stability curve for a liquid sheet. Similar results were obtained for a range in $U^*/\bar{U}_g$ of from 1 to 100.

For subsonic flow ($M = 0.7$) a similar insensitivity to gas shear was found. However, it is interesting to note that the addition of the interfacial shear imparts a wave velocity (in the downstream direction) to the liquid. This corrects the physically unrealistic inviscid gas subsonic solution (as reported in Ref. 7 and verified numerically in the present study) in which the only unstable solution for subsonic flow is that for which the wave velocity is equal to zero.

Solutions for the inviscid gas stability equation were then obtained for the fluid properties and test conditions of Tests 1–6. Figure 4 shows these results for Tests 1–4. These curves all exhibit one wavelength (λ_M) for maximum perturbation growth rate and a minimum wavelength (λ_c) below which there is no positive growth rate solution, and above which a positive growth rate always exists. For the liquids tested here carbon tetrachloride exhibits the lowest values for both λ_M and λ_c.

Finally, it is shown in Ref. 17 that by arbitrarily fixing the sheltering parameter, β at 0.85 λ_M and λ_c, as calculated for Mayer's theory, agrees remarkably well with the values ob-

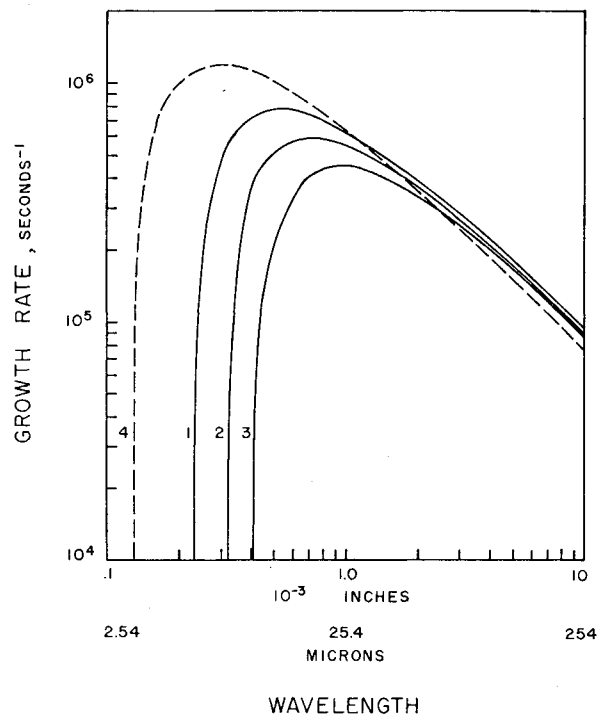

Fig. 4 Liquid stability curves with properties from sheet Tests 1–4.

tained from the linearized approach. However, there is no conceptual justification for selecting this constant and, in fact, the selected value is quite different from the value of 0.3 suggested by Mayer.

Comparison of Theory with Observations

Both the high-speed movies and photomicrographs show that, at least, the visible waves are not regular periodic curves as assumed in the analysis, but rather individual protrusions resembling sine waves terminated after half of a period. There is, therefore, a complication in comparing observed wavelengths with theoretical. In order to circumvent this difficulty it is assumed that the thickness at the base of the observed waves are indeed half of the wavelength, and thus the observed wavelengths are on the order of 300 μ. Then, from the results of the numerical calculations we see that the growth rate for perturbations with a wavelength of 300 μ is relatively large for all liquids tested. Therefore, there is agreement between theory and experiments with respect to the existence of the observed waves, assuming that the wavelength doesn't change significantly between the initial perturbation and the fully grown wave.

The calculated perturbation velocities for Tests 1, 3, and 4 are 27 fps, 18 fps, and 10 fps, respectively. The observed wave velocities from the high-speed movies were 8.2 fps, 6.1 fps, and 4.9 fps. The difference between the calculated velocity at maximum growth rate and the observed wave velocity can be attributed to either observing longer, and thus more visible, waves in the movies than those corresponding to λ_M, and/or the difference in wave velocity that would occur between the small perturbations assumed in the analysis and the finite waves observed. It is encouraging, however, that the observed and calculated velocities increase in the same direction, and are of the same order of magnitude.

From the photomicrograph results it was verified that droplets and ligaments are indeed shed from waves on the liquid surface. From the theory, any wavelength above λ_c would be capable of such action. However, it is reasonable to expect that the number of droplets shed for each wave is proportional, in some way, to the growth rate for the particular wavelength. Also, because of shedding mechanism it is ap-

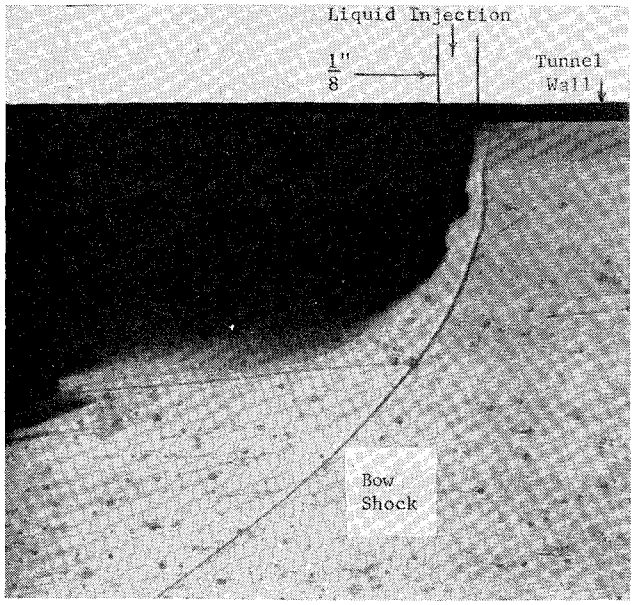

Fig. 5 Spark shadowgraph—injection of carbon tetrachloride into Mach 2.1 freestream.

parent that a droplet diameter cannot be larger than the wavelength of the parent wave. Indeed, from the pictures, the droplets and ligament diameters are some fraction (about $\frac{1}{3}$ or less) of the parent wave. Finally, from the theoretical curves in Fig. 4 then, one would expect the maximum droplet size for each test to be approximately the same, since the curves merge together as the wavelength increases.

With these ideas in mind one can compare the shape of the obtained droplet distribution histograms with what one would expect from theory. For example, the skewness of the distributions towards lower wavelengths, which was observed with all the liquids, provides excellent agreement with the hypothesis that the most frequent droplet diameter for a given liquid is some fraction of λ_M (which ranged from 7.6 μ for CCl_4 to 18.2 μ for the 20% glycerol/water solution) and that the droplet frequency, in general, is proportional to the growth rate. In addition, since the theoretical curves merge towards the right it is not surprising that (except for the test with CCl_4) there is no large scale difference in the droplet distributions. Furthermore, since carbon tetrachloride has a vapor pressure which is five times that of any other fluid tested, it is suggested that the discrepancy between theory and observations is due to either the rapid evaporation of the liquid droplets, or the effect of vapor pressure (which is ignored in the analysis) on the droplet formation. Finally, the maximum observed droplet size is the same for all liquids (100 μ range), except carbon tetrachloride, as predicted by the analysis.

III. Liquid Jets

The liquid jet testing consisted of two phases. First, spark shadowgraphs and high speed movies were taken of various liquids injected normally from a $\frac{1}{8}$ in. diameter nozzle. Second, photomicrographs were taken of the normal injection of various liquids from a 0.018 in. diam nozzle, and of water from a 0.033-in.-diam nozzle. In both cases the tests were conducted in the 6-in. supersonic wind tunnel, freestream Mach number measured 2.1, and gas stagnation pressure and temperature were at atmospheric values.

$\frac{1}{8}$ In.-Diam Jet Tests

Apparatus

For these tests the liquid was injected via an injection assembly built into the tunnel block. This assembly consists of an 8 in. long, $\frac{3}{4}$ in. i.d., straight copper feed tube inserted normally through the tunnel top to the shoulders of a brass insert which is epoxied into a counter-bored hole in the tunnel block. The $\frac{1}{8}$ in. diam brass nozzle is then screwed from the tunnel side of the block into the brass insert. Appropriate neoprene 0-rings, rubber gaskets, and clamps are provided, and an immersion-type copper-constantan thermocouple was used to measure liquid temperature prior to entrance into the nozzle.

Liquids and test conditions

A list of the liquids and test conditions for both the spark shadowgraph and high-speed movie tests is in Table 2. The physical properties of the liquids were obtained from the indicated references at the temperature recorded from the feed tube thermocouple.

Spark shadowgraph results

Figure 5 shows the results of a spark shadowgraph test with carbon tetrachloride. In this photograph the liquid is injected from the top and the gas is flowing from right to left. The drops which are evident in the photograph are caused by liquid sticking to the wind-tunnel windows, and therefore have no significance to the test.

Figure 5 shows an over-all flowfield characterized by a well-defined curved shock upstream of the jet, with a thick gas boundary layer along the tunnel block. From Schlieren photographs, boundary-layer separation appears just upstream of the jet.

The liquid surface in Fig. 5 exhibits wave motion which appears to grow in amplitude as the jet progresses downstream. This feature is consistent with the results obtained from the high-speed movies of the $\frac{1}{8}$ in. diameter jet and is discussed subsequently.

High-speed movies of jet injection

High-speed movies (7000 frames/sec) were taken of the steady-state injection of the four liquids (Table 2), and the transient development of water injection from tunnel start (after the liquid flow is nearly at steady state) to steady state. These movies, taken with a 16 mm Fastax camera, have a time slow down factor of 292 to 1 when viewed with an ordinary 16 mm projector.

The movies very lucidly reveal the mechanism of jet development and breakup. The following descriptions of these processes are based on observation of a composite 400 ft roll of the results of Tests 1, 3, and 4, and a film of the transient test with water.

Table 2 Liquid properties[21–24] and test conditions for $\frac{1}{8}$-in. diam jet tests

Test no.	Liquid	Viscosity, lb_M/ft-sec	Density, lb_M/ft^3	Surface tension, lb/ft	$\dot{m}$, lb_M/sec	V_J, fps	q_r
1	Water	0.62×10^{-3}	62.4	4.94×10^{-3}	0.36	67.9	6.2
2	20% glycerol/water solution	1.05×10^{-3}	65.5	4.90×10^{-3}	0.33	59.3	5.0
2	30% glycerol/water solution	1.51×10^{-3}	67.2	4.84×10^{-3}	0.33	57.8	4.9
4	Carbon tetrachloride	0.6×10^{-3}	99	1.82×10^{-3}	0.44	52.5	5.9

The basic mechanism of quasi-steady-state jet breakup is similar for all three liquids. This consists of small amplitude waves, spanning the jet circumference, which commence at the nozzle outlet and move rapidly in the axial direction of the jet, while growing in amplitude. At some point, usually after the jet has turned in the direction of the stream and before the amplitude of the waves is a significant fraction of the jet radius, the jet fractures at a wave trough into one or several pieces. The jet then grows again, and the process is repeated.

Figure 6 shows this sequence of events for Test 3. In these enlargements of ten consecutive frames from this test, the injection point appears in the upper left of the light area in each frame, with freestream gas flow from left to right. Thus, for example, in frame 1 the jet is seen bending in the streamwise direction across the top half of the light area, after being injected at the upper left of the light area. In frame 1 the wave motion along the jet is evident, and fracture of the jet is beginning at a wave trough. In frames 2 and 3 jet breakup is completed, and in frame 4 the jet begins to grow again. In frame 5 the jet continues to grow, with some disintegration also evident. Further growth occurs in frames 6 and 7 until, in frame 8, the jet shape again resembles the fully grown contour of frame 1, with fracture again initiating at a wave trough. In frames 9 and 10 the jet fracture is again completed. The time to complete the full jet-disintegration-full jet cycle in Fig. 6 is 1 msec, which is the elapsed time from frames 1–8. Also, it is noted that some droplet shedding is evident in frames 5–7.

Some significant differences were observed among the three tests. The most obvious of these is the much slower wave velocity and fracture rate for the test with carbon tetrachloride as compared to both Tests 1 and 3, although this wave velocity was still too high to obtain an accurate measurement from the movie. Another observed difference between Test 4 and the other two is that the carbon tetrachloride jet exhibits a much larger degree of spread, after turning in the direction of the stream. Consequently, the initial fractured pieces appear larger in this movie as compared with Tests 1 and 3. In addition, in the test with carbon tetrachloride a larger amount of vapor surrounds the jet than for the other two tests, as would be expected.

In summary, the high-speed movies show that the jet breakup is characterized by a gross fraction of the jet stream, initiated at the troughs of waves which span the jet circumference, and move axially along the jet. This model of jet breakup will be subsequently expanded upon.

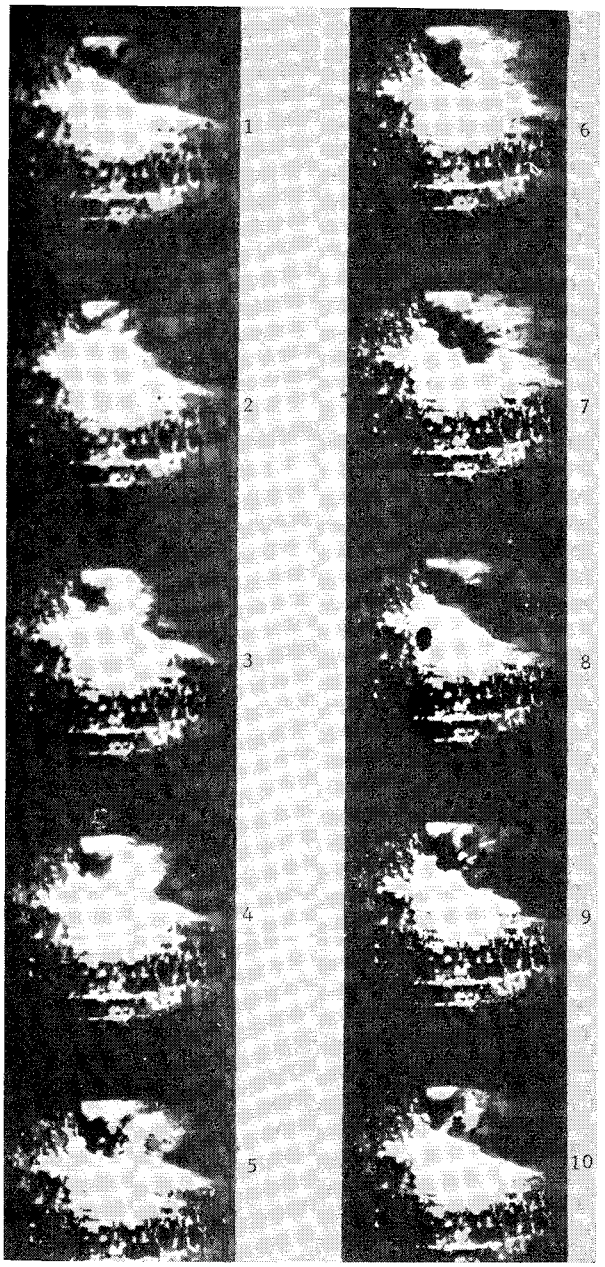

Fig. 6 Jet breakup sequence from high-speed movies; gas flow is from left to right.

Small Diameter Jet Tests

Apparatus

The model employed for this test series is a 4 in. wide by 4 in. long flat stainless steel plate with a 20° wedge angle at the leading edge. The liquid is injected into the free stream from a straight, $\frac{1}{16}$ in. long, nozzle located at the mid-span plane of the plate, 2 in. from the leading edge. The nozzle is part of a brass insert, which is removable from the bottom of the plate, and fits flush with the plate surface. The liquid is fed to this nozzle from a 2 in. diam cup-shaped settling chamber which screws to the underside of the plate, and is coaxial with the nozzle. The temperature of the liquid in the cup is measured by an immersion type copper-constantan thermocouple; the cup pressure (20–50 psig) is checked via a pressure tap and liquid pressure gage.

The optical system employed for obtaining the photomicrographs is exactly the same as was used for the liquid sheet tests.

Test liquids and conditions

Twenty tests were run in this phase of the investigation. These consisted of tests with four different liquids and a variety of flow rates with a 0.018 in. i.d. injection nozzle, and tests with water employing a 0.033 in. i.d. injection nozzle. Table 3 lists the liquids used and flow conditions for these tests. The liquid properties shown in Table 3 are representative values for each test; the liquid temperature never varied by more than a few degrees.

Results of small diameter jet tests

A representative result of the small diam jet tests is shown in Fig. 7 which is the result of Test 1d. In this photograph the liquid is injected at the bottom right and the gas flow is from right to left.

Much information about both the mechanism of jet breakup and initial droplet distributions is obtained from a close examination of the pictures obtained from these tests. However, in extracting the information, the limitations of these tests should be remembered. The primary limitation is that the test results give a detailed picture of the jet at only one instant of time. Hence, it is conceivable that at another instant of time the jet shape and particle distribution might be quite different. This is in contrast to the high-speed movies

Table 3 Liquid properties[21–24] and test conditions for small diameter jet tests

Test no.	Liquid	$\dot{m} \times 10^3$ lb/sec	V_J, fps	q_r	Viscosity, lb_M/ft-sec	Density, lb_M/ft^3	Surface tension, lb/ft
1a	Water	9.3	84.5	9.6	0.70×10^{-3}	62.4	5.0×10^{-3}
1b	Water	9.9	89.5	10.7			
1c	Water	7.1	64.2	5.6			
1d	Water	7.3	66.2	5.9			
2a	30% glycerol/water solution	8.4	70.5	7.2	2.1×10^{-3}	67.2	4.9×10^{-3}
2b	30% glycerol/water solution	10.1	85	10.5			
2c	30% glycerol/water solution	11.6	97.5	13.8			
3a	15% ethyl alcohol/H_2O solution	12	111	16.1	1.5×10^{-3}	61.6	2.9×10^{-3}
3b	15% ethyl alcohol/H_2O solution	11.6	108	16.7			
3c	15% ethyl alcohol/H_2O solution	5.4	50	3.3			
3d	15% ethyl alcohol/H_2O solution	9.4	87	9.9			
4a	Carbon tetrachloride	12.1	69.2	10.2	0.7×10^{-3}	99	1.9×10^{-3}
4b	Carbon tetrachloride	11.0	69.9	8.4			
4c	Carbon tetrachloride	8.2	46.8	4.7			
4d	Carbon tetrachloride	10.9	62.3	8.3			
4e	Carbon tetrachloride	11.7	66.9	9.5			
5a	Water	21.3	59.6	4.8	0.7×10^{-3}	62.4	5.0×10^{-3}
5b	Water	18.3	51.1	3.5			
5c	Water	15.7	44.0	2.6			
5d	Water	16.7	46.2	2.9			

Injection nozzle diameter: 0.018 in., Tests 1–4; 0.033 in., Test 5

in which the jet shape is viewed over a long period of time, but the details of the particle distributions are missing. In the discussion that follows, then, frequent reference will be made to the high-speed movies in order to develop an over-all description of jet breakup.

The following results are obtained from examination of the photographs obtained from this phase of testing: 1) Over-all Jet Surface and Breakup. The results of this phase of testing is in basic agreement with the model for jet breakup previously discussed which was based upon examination of the high-speed movies of injection from a $\frac{1}{8}$ in. diam nozzle.

This general breakup pattern is captured by several of the pictures resulting from the small diameter jet tests. For example, Test 1d lucidly illustrates this behavior. In Fig. 7 the photomicrograph from Test 1d shows the wave motion on the outside surface of the jet, with jet fracture occurring at about one third of the way in from the right side of the picture. This fracture results in large pieces of fluid leaving the jet, which are apparently in the process of breaking down into smaller particles and droplets.

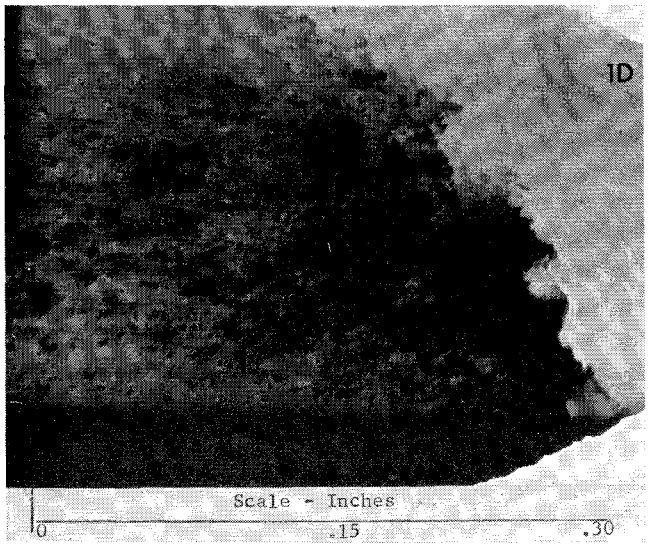

Fig. 7 Photomicrograph of water jet injection—Test 1D.

It is also noted that at the inside surface of the jets in Tests 1A, 2C, and 5A there appears to be some particle and droplet shedding before jet fracture. It is reasonable to assume that these particles are sheared off the side of the jet by the free-stream. This effect was also observed in the high-speed movies, but, apparently because of the rapidity of this droplet formation, the particles appear as streaks of fluid.

The additional details supplied by the photomicrographs can now be used to complete the basic model of jet breakup presented to this point. One addition to the model, not apparent from the movies, is that the large pieces of fluid which fracture from the jet do indeed breakdown further into smaller droplets and particles. Furthermore, nearly all of the tests show some initial droplet formation. These droplets appear to be sheared from the side and top surfaces of the jet, and thus are formed even though the main part of the jet may still be intact.

2) Effect of Liquid on Jet Shape. It was reported that the high-speed movies showed that the carbon tetrachloride $\frac{1}{8}$ in. diam jet exhibited a much larger spreading after injection than the other two liquids tested. This effect is also observed in examining the results of the photomicrograph tests of the 0.018 in. diam jet. The reason for this effect is presumed to be due to either expansion of the carbon tetrachloride vapor, and/or the low surface tension of carbon tetrachloride. However, the more important of these two properties with respect to jet spread could not be determined from this test series.

3) Degree of Jet Breakup vs Streamwise Location. Another parameter which is of interest from a combustion viewpoint is the degree of jet breakup at a given streamwise distance from the injection nozzle. The effect of the dynamic pressure ratio, and jet diameter on this parameter will now be examined.

An examination of the photographs obtained from Tests 1–5 shows that for a given fluid and injection diameter, the degree

of jet breakup at a particular streamwise location is inversely related to the dynamic pressure ratio. For example, comparison of the degree of jet breakup at the left side of the photographs from Tests 1a (high q_r) and 1d (low q_r) demonstrates this relationship. Similarly, these results were obtained in comparing the photomicrographs from 2a with 2c, 3a and 3b with 3c and 3d, 4a with 4b, and 5a with 5d. Finally, it should be noted that in comparisons between tests of the same liquid, injection diameters, andfree stream conditions, claiming that a parameter varies with q_r is equivalent to claiming that it varies with injection mass flow.

For the same q_r and fluid, the effect of increasing the jet diameter is to decrease the degree of jet breakup for a given streamwise location. This is demonstrated by comparing the photographs from Tests 5a and 1d. Since the q_r for Test 1d is actually slightly more than that for Test 5a, for the same injection diameters it would be expected that a lesser degree of breakup at a given streamwise location would be observed for Test 1d. Comparison between the two tests show, however, that the degree of breakup for Test 1d is significantly higher than for Test 5a. Similar results were found in comparing the photomicrographs from Test 5b with those from Test 1. Again, it should be noted that the correlation of the degree of jet breakup at a given streamwise location with injection diameter, as presented here, is indistinguishable from a correlation with jet flow rate.

In conclusion to the discussion of the degree of jet breakup at given streamwise location it is noted that no clearly definable relationship could be found between this parameter and injection liquid.

Droplet sizes

Droplet diameters were measured for a selected area of some of the jet photomicrographs. This area is a rectangle 1.6 in. high × 2 in. long, and bounded by the plate surface and the left side of the photograph. The droplets were measured by enlarging the selected area by a factor of 5 to 1, which results in a total magnification of 72.5, and measuring the diameters with a scale graduated in 0.10 mm. Thus, the minimum measurable interval was 6.9 μ, corresponding to a half-division on the scale. However, as with the liquid sheet tests, difficulty in distinguishing the droplets from the grain of the photograph was encountered in the 5–10 μ droplet diameter range.

The droplet diam determination obtained here has validity only as a determination of the sizes of initial droplets (i.e., droplets close to the point of injection as is the case for all of the particles in the photographs) for each test. The degree of jet breakup was not a consideration in these measurements, and may be very large (Test 1d) or very small (Test 1a). Furthermore, the downstream droplet distribution would probably be quite different, due to secondary breakup and evaporation.

The measurement was limited to particles which approximate spheres. This was arbitrarily defined as particles for which the maximum diameter does not exceed the minimum diameter by more than two to one. For the nonspherical particles thus counted, the droplet diameter was defined by (max-diam + min-diam)/2. Furthermore, only those particles and droplets that were in good focus were counted.

Under the above restrictions, then, with a sample size ranging from 83 for Test 3d to 102 for Test 5a, the mean measured droplet diameters are 58, 85, 63, 72, 58, and 68 μ, for Tests 1b, 1d, 2c, 3d, 4a, and 5a, respectively. The maximum measured droplet diameter was 352 μ, for Test 1d.

IV. Concluding Remarks

The experimental results of this investigation show that the mechanism of droplet formation from a liquid sheet exposed to a supersonic gas stream is a surface phenomenon, while the breakup of a liquid jet injected normally into a supersonic freestream is one of gross fracture of the jet. Further investigations are warranted in order to determine the effect of a high liquid vapor pressure on jet breakup, and to refine droplet distribution measurements for both problems.

References

[1] Kelvin, Lord, "Influence of Wind and Capillarity on Waves Supposed Frictionless," *Mathematical and Physical Papers*, Cambridge University Press, Vol. IV, 1910, pp. 76–86.

[2] Jeffreys, H., "On the Formation of Water Waves by Wind," *Proceedings of Royal Society of London*, Vol. 107, 1925, pp. 189–205.

[3] Taylor, G., "Effect of Variation in Density on the Stability of Superposed Streams of Fluid," *Proceedings of Royal Society*, Vol. A132, 1931, pp. 499–523.

[4] Taylor, G., "The Instability of Liquid Surfaces When Accelerated in a Direction Perpendicular to their Plans. I," *Proceedings of Royal Society of London*, Vol. A201, 1950, pp. 192–196.

[5] Lamb, H., *Hydrodynamics*, 6th ed., Dover, New York, 1945, pp. 370–378.

[6] Mayer, E., "Theory of Liquid Atomization in High Velocity Gas Streams," *ARS Journal*, Vol. 31, 1961, pp. 1783–1785.

[7] Chang, I-D. and Russel, P., "Stability of Liquid Layer Adjacent to a High-Speed Gas Stream," *The Physics of Fluids*, Vol. 8, 1965, pp. 1018–1026.

[8] Rayleigh, Lord, "On the Question of the Stability of the Flow of Fluids," *Philosophical Magazine*, Vol. XXXIV, No. 59, 1892, pp. 59–70.

[9] Rayleigh, Lord, "On the Instability of Jets," *Proceedings of London Mathematical Society*, Vol. X, No. 4, 1878, pp. 4–13.

[10] Tomotika, S., "On the Instability of a Cylindrical Thread of a Liquid Surrounded by Another Viscous Fluid," *Proceedings of the Royal Society of London*, Vol. A150, 1935, pp. 322–337.

[11] Castleman, R., "The Mechanism of Atomization of Liquids," *Journal of Research of the Bureau of Standards*, Vol. 6, 1931, pp. 369–376.

[12] Lee, D. and Spencer, R., "Preliminary Photomicrographic Studies of Fuel Sprays," TN 424, 1932, NACA.

[13] Ingebo, R., "Vaporization Rates and Drag Coefficients for Isooctane Sprays in Turbulent Air Streams," TN 3265, 1954, NACA.

[14] Foster, H. and Ingebo, R., "Evaporation of JP-5 Fuel Sprays in Air Streams," RM E55K02, 1956, NACA.

[15] Clark, B., "Breakup of a Liquid Jet in Transverse Flow of Gas," TN D-2424, 1964, NASA.

[16] Adelberg, M., "Breakup and Penetration of a Liquid Jet in a Gas Stream," *AIAA Journal*, Vol. 5, No. 8, Aug. 1967, pp. 1408–1415.

[17] Sherman, A., "An Investigation into the Breakup of Liquid Sheets and Jets in a Supersonic Gas Stream," Ph.D. dissertation, Aug. 1969, Univ. of Maryland.

[18] Wilson, A. and Chang, I-D., "Comments on Stability of a Liquid Layer Adjacent to a High-Speed Gas Stream," *The Physics of Fluids*, Vol. 10, 1967, pp. 2285–2288.

[19] Lubard, S. and Schetz, J., "Atomization and Vaporization of a Liquid Sheet Exposed to a Supersonic Stream," AIAA Paper 68-643, Cleveland, Ohio, 1968.

[20] Schlicting, H., *Boundary Layer Theory*, McGraw-Hill, New York, 1968, p. 321.

[21] Mellan, I., *Industrial Solvents*, Reinhold, New York, 1950.

[22] Chemical Rubber Co., *Handbook of Chemistry and Physics*, 46th ed., Chemical Rubber Publishers, Cleveland, 1965, pp. D110, E25, F36–38.

[23] Gebhardt, B., *Heat Transfer*, McGraw-Hill, New York, 1961, p. 431.

[24] Lay, J., *Thermodynamics*, Charles Merrill Books, Columbus, 1963, p. 808.